Proceedings of the 2014 IEEE
International Conference on Robotics and Biomimetics
December 5-10, 2014, Bali, Indonesia

Design of a Hyper-Redundant Continuum Manipulator for Intra-Cavity Tasks

Kai Xu, *Member, IEEE*, Wukun Mei, Zhixiong Yang,
Liangliang Han, and Xiangyang Zhu, *Member, IEEE*

***Abstract*—Slim and strong hyper-redundant manipulators with long reaches can perform a variety of intra-cavity tasks in confined spaces. Benefiting from a newly developed continuum mechanism and its actuation scheme, this paper proposes the design of a hyper-redundant continuum manipulator with 12 DoFs (Degrees of Freedom). With a structure synthesized in an enumerative manner, the manipulator is expected to navigate through arrays of holes to perform inspections or manipulations at remote locations in a deep cavity. Kinematics modeling, simulations, and system descriptions are elaborated. A prototype is to be constructed to experimentally verify the proposed functions of the proposed continuum manipulator.**

I. Introduction

SLIM and strong hyper-redundant manipulators with long reaches can perform a variety of intra-cavity tasks in confined spaces, such as inspection, foreign objects extraction, structure modification, manipulation, assembling, etc.

Research on such a hyper-redundant manipulator could be traced back to the 1960s when Anderson and Horn developed the hyper-redundant Tensor Arm manipulator [1]. Since then, many hyper-redundant manipulators were developed [2-11].

Mainly three approaches were followed to design these hyper-redundant manipulators.

- ✧ A hyper-redundant manipulator is formed by several serially connected modules (e.g., the ones in [2, 3]). Each module has one or two DoFs with actuators integrated inside the module. The main issue is the number of stackable modules is limited, since the distal modules become overhead loads of the proximal ones.
- ✧ Cable actuation is used for a hyper-redundant manipulator [4-7]. The main issue lies on the tension control of these actuation cables. When the manipulator is driven into a complex spatial shape, maintaining the tensions on the cables can be quite challenging, given unavoidable cable elongation and friction.
- ✧ Elastic materials (e.g. rubber and silicone) are used to form soft hyper-redundant manipulators [8-11]. These soft manipulators are driven by pneumatic or hydraulic pressure differentials. Payload and positioning accuracy could be of concerns for these designs.

Inspired by the continuum surgical robots with multiple backbones and push-pull actuation as in [12-15], this paper proposes to design a hyper-redundant continuum manipulator with 12 DoFs as shown in Fig. 1. With a structure carefully synthesized in an enumerative manner, the manipulator is expected to navigate through arrays of holes to perform inspections or manipulations at remote locations in a deep cavity. Benefitting from a newly developed modular actuation scheme for the multi-backbone continuum robot, this hyper-redundant continuum manipulator is expected to be more easily controlled than the cable-driven manipulators, as well as provide higher payload capabilities and better positioning accuracies than the soft hyper-redundant manipulators.

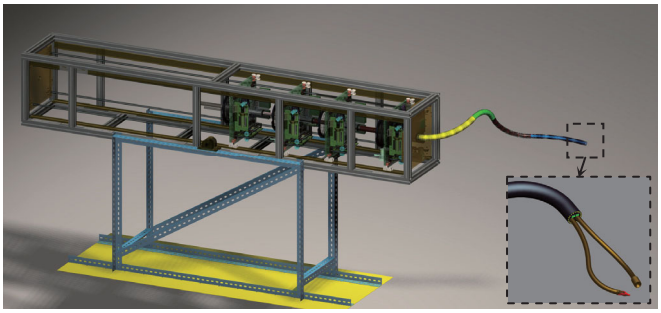

Fig. 1. Design of the hyper-redundant continuum manipulator

Main contributions of this paper include the proposed design of this hyper-redundant continuum manipulator for intra-cavity tasks, including the structure synthesis and the detailed component designs.

This paper is organized as follows. Section II presents the design overview. Kinematics-based structure synthesis and simulations of the manipulator is presented in Section III Section IV describes the actuation scheme and various system components in detail. Conclusions and future works are summarized in Section V.

Manuscript received July 31, 2014. This work was supported in part by the Joint Research Center of Advanced Aerospace Technology (Grant No. USCAST2013-17), in part by the State Key Laboratory of Mechanical Systems and Vibration (Grant No. MSVZD201406), and in part by the National Natural Science Foundation of China (Grant No. 51375295).

Kai Xu is with the RII Lab (Lab of Robotics Innovation and Intervention), UM-SJTU Joint Institute, Shanghai Jiao Tong University, Shanghai, 200240, China (corresponding author, phone: 8621-34207220; fax: 8621-34206525; email: k.xu@sjtu.edu.cn).

Wukun Mei is with the RII Lab (Lab of Robotics Innovation and Intervention), UM-SJTU Joint Institute, Shanghai Jiao Tong University, Shanghai, China (email: meiwk1005@sjtu.edu.cn).

Zhixiong Yang is with the RII Lab (Lab of Robotics Innovation and Intervention), UM-SJTU Joint Institute, Shanghai Jiao Tong University, Shanghai, China (email: yangzhixiong@sjtu.edu.cn).

Liangliang Han is with Institute of Aerospace System Engineering, Shanghai, China.

Xiangyang Zhu is with the School of Mechanical Engineering, Shanghai Jiao Tong University, Shanghai, China (email: mexyzhu@sjtu.edu.cn).

978-1-4799-7397-2/14/$31.00 © 2014 IEEE

II. Design Overview

The design of the proposed manipulator is inspired by the multi-backbone continuum robot as in [12-15]. The manipulator is expected to reach various remote locations in a deep cavity with complex internal structures. Due to the particular arrangement of the mockup cavity as detailed in Section III.C, the continuum manipulator is expected to have four segments, as shown in Fig. 2.

Each segment that is also depicted in Fig. 3 has three DoFs (2-DoF bending plus 1-DoF extension/contraction). The segments are assumed to have circular shapes according to the theoretic and experimental studies as in [16, 17]. The structure synthesis presented in Section III.C is based on this assumption. Then kinematics simulations are presented in Section III.D to verify whether the synthesized manipulator structure is suitable for the intended task of exploring the cavity and reaching the desired remote locations.

Using the concept of a dual continuum mechanism as explained in Section IV.A, the manipulator is designed with the descriptions elaborated in Section IV.

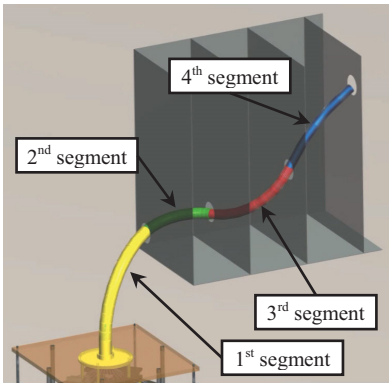

Fig. 2. Design overview of the hyper-redundant continuum manipulator

III. Kinematics-Based Structure Synthesis

The proposed continuum manipulator consists of four segments. Each segment depicted in Fig. 3 consists of a base ring, several spacers, an end ring, and several backbones. The backbones are all made from super-elastic nitinol rods. Pushing and/or pulling these backbones drives one segment: differentially pushing and pulling realizes a 2-DoF bending, whereas synchronously pushing or pulling realizes a 1-DoF elongation/compression of each segment. The spacer rings are distributed evenly along one segment to prevent the buckling of the backbones.

With nomenclature and coordinates defined, the kinematics is derived. Then structure synthesis and simulations are reported in Section III.C and Section III.D.

A. Nomenclatures and Coordinates

The t^{th} segment ($t = 1,2,3,4$) is shown in Fig. 3, whereas the nomenclatures are defined in Table I. Coordinate systems of the t^{th} segment are defined as below:

- *Base Ring Coordinate*, $\{tb\} \equiv \{\hat{\mathbf{x}}_{tb}, \hat{\mathbf{y}}_{tb}, \hat{\mathbf{z}}_{tb}\}$, is attached to the base ring of the t^{th} segment. $\hat{\mathbf{x}}_{tb}$ points from the center to the first backbone while $\hat{\mathbf{z}}_{tb}$ is normal to the base ring. Backbones are numbered consistently with δ_{ti}.
- *Bending Plane Coordinate 1*, $\{t1\} \equiv \{\hat{\mathbf{x}}_{t1}, \hat{\mathbf{y}}_{t1}, \hat{\mathbf{z}}_{t1}\}$, shares its origin with $\{tb\}$ and has the continuum segment bending in its XZ plane.
- *Bending Plane Coordinate 2*, $\{t2\} \equiv \{\hat{\mathbf{x}}_{t2}, \hat{\mathbf{y}}_{t2}, \hat{\mathbf{z}}_{t2}\}$, is obtained from $\{t1\}$ by a rotation about $\hat{\mathbf{y}}_{t1}$. $\hat{\mathbf{z}}_{t1}$ is normal to the end ring with the origin of $\{t2\}$ located at the end ring's center.
- *End Disk Coordinate*, $\{te\} \equiv \{\hat{\mathbf{x}}_{te}, \hat{\mathbf{y}}_{te}, \hat{\mathbf{z}}_{te}\}$, is fixed to the end ring of the t^{th} segment. $\hat{\mathbf{x}}_{te}$ points from center to the first backbone and $\hat{\mathbf{z}}_{te}$ is normal to the end ring. $\{te\}$ is obtained from $\{t2\}$ by a rotation about $\hat{\mathbf{z}}_{t2}$.

When the t^{th} and $(t+1)^{\text{th}}$ segments are stacked, $\{te\}$ coincides with $\{(t+1)b\}$.

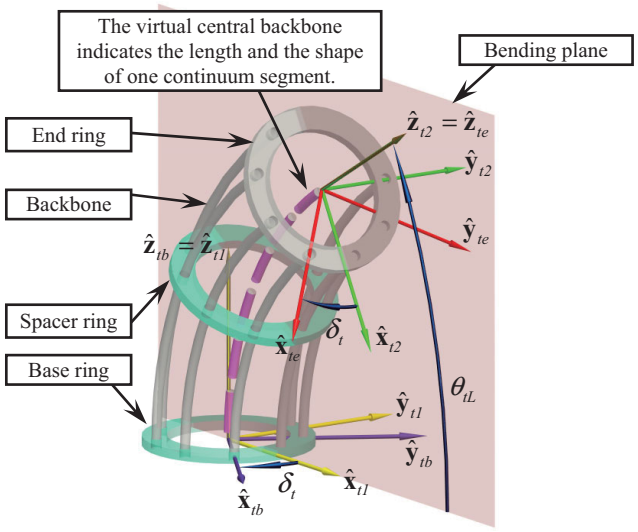

Fig. 3. Nomenclatures and coordinates of the t^{th} segment

TABLE I
Nomenclature Used in This Paper

i	Index of the backbones, $i = 1,2,\cdots,m$
t	Index of the segments $t = 1,2,\ldots,n$; numbering of the segments always precedes the backbones.
r_{ti}	Radius of the pitch circle defining the positions of the i^{th} backbone in all the rings of the t^{th} segment.
β_{ti}	Division angle of the i^{th} backbone along the circumference of the pitch circle.
L_t, L_{ti}	Length of the virtual central backbone and the i^{th} backbone for the t^{th} segment
$\theta_t(s)$	The angle of the tangent to the virtual central backbone in the bending plane for the t^{th} segment. $\theta_t(L_t)$ and $\theta_t(0)$ are denoted by θ_{tL} and θ_0. $\theta_0 = \pi/2$ is a constant.
δ_{ti}	For the t^{th} segment, a right-handed rotation angle from $\hat{\mathbf{x}}_{t1}$ about $\hat{\mathbf{z}}_{t1}$ to a ray passing through the i^{th} backbone.
δ_t	$\delta_t \equiv \delta_{t1}$ and $\delta_{ti} = \delta_t + \beta_{ti}$

$\boldsymbol{\psi}_t$	$\boldsymbol{\psi}_t = [\theta_{tL} \;\; \delta_t \;\; L_t]^T$ is a configuration vector which defines the status of the t^{th} segment.
${}^{1}\mathbf{R}_{2}$	Coordinate transformation matrix frame *2* to frame *1*.
${}^{tb}\mathbf{p}_t(s)$	Position vector of a point along the central backbone in $\{tb\}$. ${}^{tb}\mathbf{p}_t(L_t)$ is the tip position designated by ${}^{tb}\mathbf{p}_{tL}$.

B. Kinematics of the t^{th} Segment

Thorough derivation of the kinematics of one continuum segment can be found in [13, 17-19]. Related entities are summarized here. Kinematics of the t^{th} segment will be used for the structure synthesis in Section III.C.

The length and the shape of the t^{th} continuum segment can be indicated by virtual central backbone and parameterized by the configuration vector $\boldsymbol{\psi}_t = [\theta_{tL} \;\; \delta_t \;\; L_t]^T$.

The experimentally proven assumption that the segment bends into a circular shape [16, 17] gives the following.

$$ {}^{tb}\mathbf{p}_{tL} = \frac{L_t}{\theta_{tL} - \theta_0} \begin{bmatrix} \cos\delta_t (\sin\theta_{tL} - 1) \\ \sin\delta_t (1 - \sin\theta_{tL}) \\ -\cos\theta_{tL} \end{bmatrix} \tag{1} $$

Where ${}^{tb}\mathbf{p}_{tL} = [0 \;\; 0 \;\; L_t]^T$ when $\theta_{tL} = \theta_0 = \pi/2$

${}^{tb}\mathbf{R}_{te}$ associates $\{te\}$ and $\{tb\}$.

$$ {}^{tb}\mathbf{R}_{te} = \mathrm{R}(\hat{\mathbf{z}}_{tb}, -\delta_t)\,\mathrm{R}(\hat{\mathbf{y}}_{t1}, \theta_0 - \theta_{tL})\,\mathrm{R}(\hat{\mathbf{z}}_{t2}, \delta_t) \tag{2} $$

Where $\mathrm{R}(\hat{\mathbf{n}}, \gamma)$ designates rotation about $\hat{\mathbf{n}}$ by an angle γ.

Length of the t^{th} backbone can be written as:

$$ L_{ti} = L_t + r_{ti}\cos\delta_{ti}(\theta_{tL} - \theta_0) \tag{3} $$

C. Structure Synthesis

The mockup cavity is shown in Fig. 4. There are four arrays of holes which allow the manipulator to pass. The continuum manipulator is expected to enter the cavity at the $[0 \;\; 0 \;\; 0]^T$ point and reach every hole in the fourth array. The distance between the arrays varies between 110mm and 150mm. Within one array, the distance between the vertical and horizontal adjacent holes is 80mm. The arrays are also shifted for 40mm both in the horizontal and the vertical directions so that the holes in the 1st and 2nd arrays are not co-axial. The 3rd and the 4th arrays have the same amount of offsets.

The structure synthesis is performed to generate proper parameters of the manipulator so that the holes in the 4th array could all be reached.

Although the kinematics for hyper-redundant manipulators was obtained in [20], it doesn't lead to direct solution of this structure synthesis problem. This paper used an enumerative approach for the synthesis.

It was assumed holes in the t^{th} array will be reached by the t^{th} segment. This is a conservative assumption since it is possible for the *1*st segment to reach a hole in the *2*nd array.

As shown in Fig. 4, when the P_1 point is to be reached by the *1*st segment, a desired configuration of the *1*st segment $\boldsymbol{\psi}_1 = [\theta_{1L} \;\; \delta_1 \;\; L_1]^T$ can be solved by the following equation:

$$ {}^{1b}\mathbf{p}_{1L} = \frac{L_1}{\theta_{1L} - \theta_0} \begin{bmatrix} \cos\delta_1 (\sin\theta_{1L} - 1) \\ \sin\delta_1 (1 - \sin\theta_{1L}) \\ -\cos\theta_{1L} \end{bmatrix} = {}^{1b}\begin{bmatrix} P_{1x} \\ P_{1y} \\ P_{1z} \end{bmatrix} \tag{4} $$

Where ${}^{1b}[P_{1x} \;\; P_{1y} \;\; P_{1z}]^T$ is the coordinates of P_1 in $\{1b\}$.

Then when the P_2 point is to be reached by the *2*nd segment, the desired configuration $\boldsymbol{\psi}_2 = [\theta_{2L} \;\; \delta_2 \;\; L_2]^T$ can be solved from Eq. (5).

$$ {}^{2b}\mathbf{p}_{2L} = \frac{L_2}{\theta_{2L} - \theta_0} \begin{bmatrix} \cos\delta_2 (\sin\theta_{2L} - 1) \\ \sin\delta_2 (1 - \sin\theta_{2L}) \\ -\cos\theta_{2L} \end{bmatrix} = {}^{2b}\begin{bmatrix} P_{2x} \\ P_{2y} \\ P_{2z} \end{bmatrix} \tag{5} $$

Where ${}^{2b}[P_{2x} \;\; P_{2y} \;\; P_{2z}]^T$ is the coordinates of P_2 in $\{2b\}$ and it could be obtained by Eq. (6).

$$ {}^{2b}\begin{bmatrix} P_{2x} \\ P_{2y} \\ P_{2z} \end{bmatrix} = \left({}^{1b}\mathbf{R}_{2b}\right)^{-1} \left({}^{1b}\begin{bmatrix} P_{2x} \\ P_{2y} \\ P_{2z} \end{bmatrix} - {}^{1b}\mathbf{p}_{1L} \right) \tag{6} $$

Where ${}^{1b}[P_{2x} \;\; P_{2y} \;\; P_{2z}]^T$ is the coordinates of P_2 in $\{1b\}$ and it is known once the cavity is constructed.

In order to reach certain points in the *3*rd and *4*th arrays, the configuration of the *3*rd and *4*th segments could be obtained similarly.

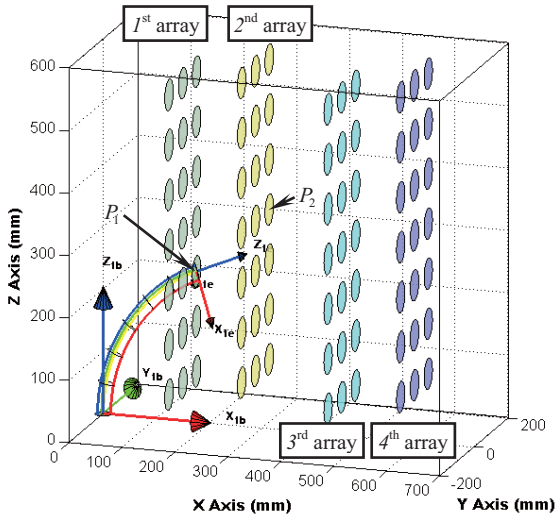

Fig. 4. The mockup cavity and Design

It is preferred to find out an optimized structure of the continuum manipulator such as with minimal L_t ($t = 1, 2, 3, 4$) values, all the holes in the *4*th array would be reached by the proposed manipulator.

The optimization is conducted in an enumerative manner, which means all possible configurations of the manipulator is generated by enumerating different combinations of reaching a certain hole in one of the four arrays.

A configuration of the manipulator is invalidated if any segment exceeds a 90-degree bending. Then among all the

possible configurations, the one with a smallest L_t value is eventually selected. By rounding the L_t values, the parameters of the manipulation are decided as in Table II.

D. Kinematics Simulations

The structure synthesis process is an algebraic process. Kinematics simulations were conducted to verify the structure synthesis results.

When the distances between the adjacent hole arrays varies between 110mm and 150mm, the holes in the 4^{th} array can always be reached, using the structural parameters from Table II. A few representative configurations for reaching the holes are shown in Fig. 5.

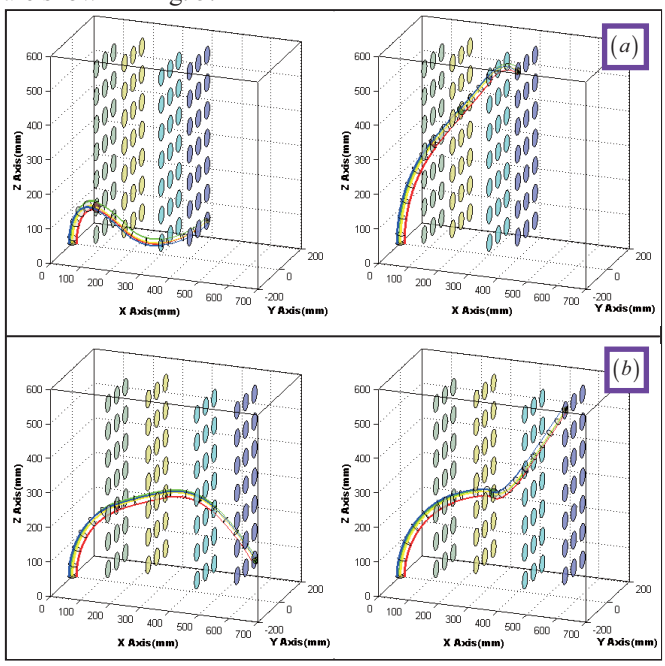

Fig. 5. Holes reached for (a) 110mm and (b) 150mm array intervals

IV. System Design Descriptions

With the manipulator structure synthesized in Section III, Section IV reports the design of the manipulator which aims at realizing the reaching motions.

A. Dual Continuum Mechanism

Each backbone in the segment as shown in Fig. 3 might need to be pushed or pulled by one motorized lead screw according to the actuation kinematics as in Eq. (3). Since more backbones are desired for a better mechanical performance and each segment possesses only three DoFs, it doesn't seem smart to use ten servo motors and lead screws to drive a segment with ten backbones.

A modular actuation scheme is hence introduced by using the dual continuum mechanism as shown in Fig. 6. The dual continuum mechanism consists of i) a distal continuum segment, ii) a proximal continuum segment, and iii) a set of rigid guiding cannulae. Both the distal segment and the proximal segment have a structure similar to the one shown in Fig. 3. A nitinol rod as a backbone is attached to the end ring of the distal segment. Then the backbone is routed through the distal segment, the guiding cannula, the proximal segment and connected to the end ring of the proximal segment. The arrangement of the backbones in the distal segment is similar and scaled to that of the proximal segment. Hence bending of the proximal segment bends the distal segment in the opposite direction.

An actuation continuum segment with four backbones is shown in Fig. 6(b). It could be bent by pushing and pulling these backbones. The dual continuum mechanism shown in Fig. 6(a) could be assembled into the actuation continuum segment so that the actuation segment deforms the proximal segment so as to drive the distal segment, no matter how many backbones are there in the distal continuum segment.

This actuation scheme introduces the structure modularity. Distal segments with different dimensions could be paired to the same proximal segment so that one actuation segment could drive various distal segments.

If the distal segment is partially housed in a tube, the part in the tube would be forced straight. The rest part would still be bent but the effective length of the segment is reduced. Using this approach, the 3^{rd} DoF of the distal segment could be realized by keeping the distal segment in a housing and translating the entire dual continuum mechanism.

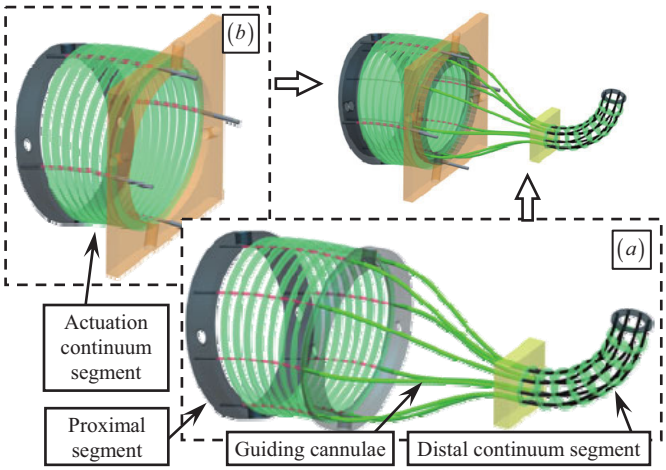

Fig. 6. A module actuation scheme: (a) a dual continuum mechanism and (b) an actuation continuum segment

B. Design Descriptions

Following the concept of the dual continuum mechanism, the continuum manipulator is designed as in Fig. 7, whereas the modular actuation unit is shown in Fig. 8. The manipulator could be assembled into the actuation unit as shown in Fig. 1. A hollow channel is reserved in the manipulator so that an endoscope and/or additional tools should be delivered to the remote site, as shown in the inset of Fig. 1.

The continuum manipulator in Fig. 7 consists of 4 sets of the dual continuum mechanisms. The distal segments of these dual continuum mechanisms are all designed to be long enough. The 4^{th} distal segment could be completely housed inside the 3^{rd} segment. The 4^{th} distal segment can be pushed

out and bent so that the effective length of the 4th segment varies between 0mm and 450mm. Then the 3rd distal segment is housed inside the 2nd segment, whereas the 2nd segment is housed inside the 1st segment.

The 1st segment has an outer diameter of 30mm and an inner diameter of 26.4mm. The 2nd, 3rd and 4th segments have outer diameters of 25mm, 20mm, and 15 mm, and inner diameters of 21.4mm, 16.4mm, and 11.4 mm, respectively. A Ø10mm endoscope or a thinner endoscope with a few tools can be easily housed inside the 4th distal segment. Other structural parameters of the distal segments are listed in Table II.

A braided stainless steel overtube shown in the inset of Fig. 7 is used to cover each distal segment. These stainless steel overtubes can enhance the torsional rigidity of the distal segments without compromising their bending capabilities. The overtubes also provide smooth surfaces to facilitate the relative translations of the distal segments.

The four proximal segments are identical with outer diameters of 135mm, and inner diameters of 125mm.

20 backbones are routed from the end ring of the distal segment to the end ring of the corresponding proximal segment through a set of 20 cannulae. The backbones are made from super-elastic nitinol with diameters of 0.7mm. The cannulae have outer diameters of 1.1mm and inner diameters of 0.9mm. The two ends of each cannula are soldered to the base rings of the corresponding distal and proximal segments so that motions of the proximal segment could be faithfully transmitted to those of the distal segment.

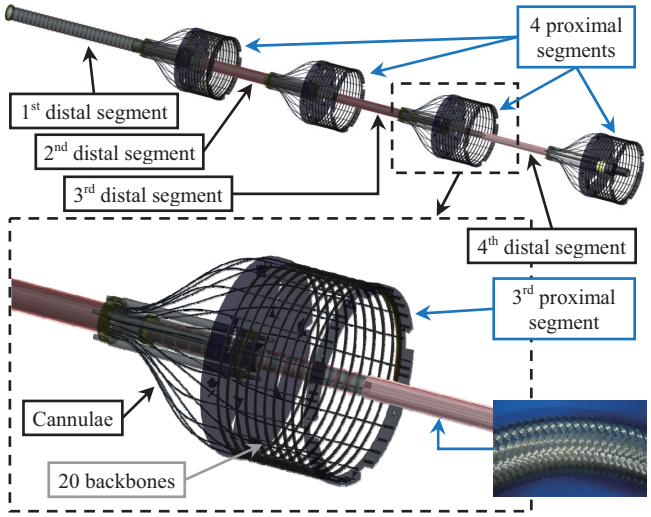

Fig. 7. Design of the continuum manipulator

TABLE II
STRUCTURE PARAMETERS OF THE MANIPULATOR

$\theta_{tL} \in [0, \pi/2]$	$\delta_t \in [-\pi, \pi]$		$L_t \in [0, 450mm]$
$r_{1i} = 14.1mm$	$r_{2i} = 11.6mm$	$r_{3i} = 9.1mm$	$r_{1i} = 6.6mm$

The actuation unit in Fig. 8 consists of four identical sets of actuation segments. Each segment has an outer diameter of 155mm, an inner diameter of 136mm and a matching length of the proximal segments. Four backbones are attached to the end ring of each actuation segment. The four backbones are arranged 90° apart along a circle with a diameter of 140mm. According to the actuation kinematics as in Eq. (3), the same amount of pushing and pulling is needed for the two opposite backbones (e.g., the two that are located 180° away from each other) to bend the actuation segment. A motorized ball screw is designed to push and pull the two backbones for the same amount. The ball screw has a diameter of 6mm, a lead of 2mm and an effective travel of 90mm. Namely two motorized ball screws drive the bending motions of the actuation segment so as to bend the corresponding proximal and distal segments.

Each actuation segment uses four sliding bushing to guide its translations with respect to one another. The translations are realized by motorized Ø12mm ball screws with a lead of 2mm. In order to minimize the bending of the guiding shafts, each segment is also equipped with four sets of rollers which roll inside rails that are installed on the frame of the system.

For each actuation segment, a WXY10 linear potentiometer with a travel of 600mm is used to measure the absolute translation between the adjacent actuation segments. Two KTL linear potentiometers with a travel of 100mm are used to measure the absolute amount of pushing and pulling of the backbones.

One fabricated and assembled actuation segment is shown in the inset of Fig. 8.

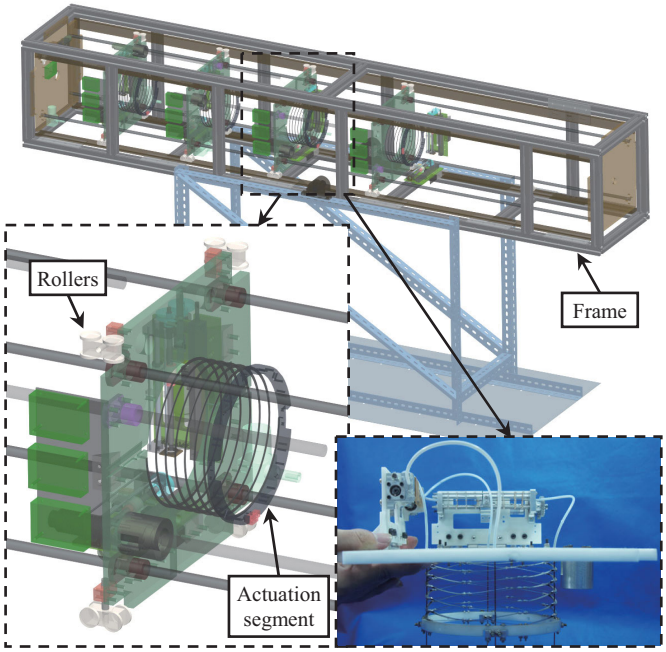

Fig. 8. Design of the actuation unit with one fabricated subassembly

Control infrastructure of the continuum manipulator is planned as shown in Fig. 9.

Twelve servomotors would be used to drive the four sets actuation segments in the actuation unit. The servomotors are the DCX22L motors from Maxon Inc. with the GPX-22 gearheads with a gear ratio of 21:1, and the ENX16 encoders with 512 CPT (Counts per Turn). Twelve Maxon EPOS2 24/2 digital controllers are used to control the servomotors.

Desired positions are transmitted from the central controller to the EPOS2 controllers via CAN buses every 2ms.

The central controller in Fig. 9 is a Cortex-A8 embedded system (TQ_AM335X from Guangzhou Embedsky Computer Technology Co., Ltd). It is equipped with a 7-inch Capacitive Touch Screen, a 1GHz CPU and two channels of CAN transceivers. Each CAN channel communicates with six EPOS2 controllers.

A user operates a 3D joystick to control the motion of each segment, since each segment has three DoFs. The proposed scheme for user inputs is to control the segments one by one. Modifications of the user input scheme will be proposed once this method is found to be counterintuitive to a user.

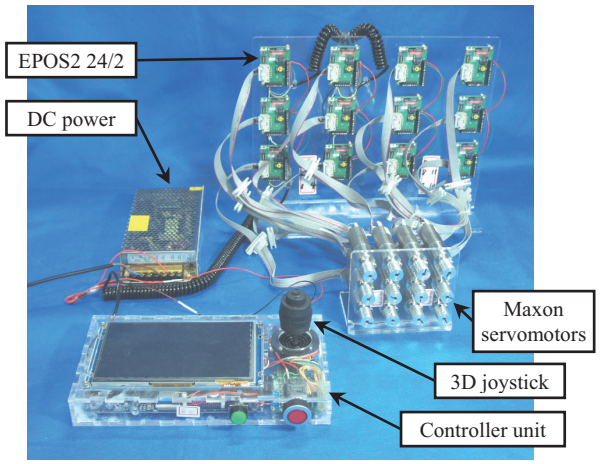

Fig. 9. The control and drive infrastructure

V. Conclusion

This paper reports the design of a 12-DoF hyper-redundant continuum manipulator.

Based on a kinematics model, the manipulator's structure is synthesized in an enumerative manner. Simulations were performed to confirm its capability of navigating through four arrays of holes to reach remote locations in a deep cavity.

Using the concept of the dual continuum mechanisms, the design of the continuum manipulator was materialized. Details of the manipulator, its actuation scheme and control infrastructure are presented.

A hollow channel is reserved in the center of this long and slim manipulator. An endoscope and/or miniature tools can be deployed to perform inspections or manipulations tasks. A prototype is to be constructed to experimentally verify the proposed functions of this continuum manipulator.

References

[1] V. C. Anderson and R. C. Horn, "Tensor Arm Manipulator." vol. 3,497,083, U. S. P. Office, Ed. United States, 1970.

[2] E. Paljug, T. Ohm, and S. Hayati, "The JPL Serpentine Robot: a 12 DOF System for Inspection," in *IEEE International Conference on Robotics and Automation (ICRA)*, Washington, DC, 1995, pp. 3143-3148.

[3] A. Wolf, H. B. Brown, R. Casciola, A. Costa, M. Schwerin, E. Shamas, and H. Choset, "A Mobile Hyper Redundant Mechanism for Search and Rescue Tasks," in *IEEE/RSJ International Conference on Intelligent Robots and Systems (IROS)*, Las Vegas, Nevada, 2003, pp. 2889-2895.

[4] S. Hirose and S. Ma, "Coupled Tendon-Driven Multijoint Manipulator," in *IEEE International Conference on Robotics and Automation (ICRA)*, Sacramento, CA, USA, 1991, pp. 1268-1275.

[5] S. Ma, I. Kobayashi, S. Hirose, and K. Yokoshima, "Control of a Multijoint Manipulator "Moray Arm"," *IEEE/ASME Transactions on Mechatronics,* vol. 7, No.3, pp. 304-317, Sep 2002.

[6] R. Buckingham, V. Chitrakaran, R. Conkie, G. Ferguson, A. Graham, A. Lazell, M. Lichon, N. Parry, F. Pollard, A. Kayani, M. Redman, M. Summers, and B. Green, "Snake-Arm Robots: A New Approach to Aircraft Assembly," in *SAE Aerotech Congress*, Los Angeles, CA, USA, 2007.

[7] R. Buckingham and A. Graham, "Nuclear Snake-Arm Robots," *Industrial Robot: An International Journal,* vol. 39, No.1, pp. 6-11, 2012.

[8] K. Suzumori, S. Iikura, and H. Tanaka, "Development of Flexible Microactuator and Its Applications to Robotic Mechanisms," in *IEEE International Conference on Robotics and Automation (ICRA)*, Sacramento, CA, USA, 1991, pp. 1622-1627.

[9] W. McMahan, V. Chitrakaran, M. Csencsits, D. M. Dawson, I. D. Walker, B. A. Jones, M. Pritts, D. Dienno, M. Grissom, and C. D. Rahn, "Field Trials and Testing of the OctArm Continuum Manipulator," in *IEEE International Conference on Advanced Robotics (ICAR)*, Orlando, FL, USA, 2006, pp. 2336-2341.

[10] J. Yang, P. Jason, and K. Abdel-Malek, "A Hyper-Redundant Continuous Robot," in *IEEE International Conference on Robotics and Automation (ICRA)*, Orlando, Florida, USA, 2006, pp. 1854-1859.

[11] M. Rolf and J. J. Steil, "Constant Curvature Continuum Kinematics as Fast Approximate Model for the Bionic Handling Assistant," in *IEEE/RSJ International Conference on Intelligent Robots and Systems (IROS)*, Vilamoura, Algarve, Portugal, 2012, pp. 3440-3446.

[12] N. Simaan, K. Xu, A. Kapoor, W. Wei, P. Kazanzides, P. Flint, and R. H. Taylor, "Design and Integration of a Telerobotic System for Minimally Invasive Surgery of the Throat " *International Journal of Robotics Research,* vol. 28, No.9, pp. 1134-1153, 2009.

[13] K. Xu and N. Simaan, "Intrinsic Wrench Estimation and Its Performance Index of Multi-Segment Continuum Robots," *IEEE Transactions on Robotics,* vol. 26, No.3, pp. 555-561, June 2010.

[14] J. Zhao, X. Zheng, M. Zheng, A. J. Shih, and K. Xu, "An Endoscopic Continuum Testbed for Finalizing System Characteristics of a Surgical Robot for NOTES Procedures," in *IEEE/ASME International Conference on Advanced Intelligent Mechatronics (AIM)*, Wollongong, Australia, 2013, pp. 63-70.

[15] J. Ding, R. E. Goldman, K. Xu, P. K. Allen, D. L. Fowler, and N. Simaan, "Design and Coordination Kinematics of an Insertable Robotic Effectors Platform for Single-Port Access Surgery," *IEEE/ASME Transactions on Mechatronics,* vol. 18, No.5, pp. 1612-1624, Oct 2013.

[16] K. Xu and N. Simaan, "Analytic Formulation for the Kinematics, Statics and Shape Restoration of Multibackbone Continuum Robots via Elliptic Integrals," *Journal of Mechanisms and Robotics,* vol. 2, No.011006, pp. 1-13, Feb 2010.

[17] K. Xu and N. Simaan, "An Investigation of the Intrinsic Force Sensing Capabilities of Continuum Robots," *IEEE Transactions on Robotics,* vol. 24, No.3, pp. 576-587, June 2008.

[18] B. A. Jones and I. D. Walker, "Kinematics for Multisection Continuum Robots," *IEEE Transactions on Robotics and Automation,* vol. 22, No.1, pp. 43-55, Feb 2006.

[19] R. J. Webster and B. A. Jones, "Design and Kinematic Modeling of Constant Curvature Continuum Robots: A Review " *International Journal of Robotics Research,* vol. 29, No.13, pp. 1661-1683, Nov 2010.

[20] G. S. Chirikjian, "Hyper-Redundant Manipulator Dynamics: A Continuum Approximation," *Advanced Robotics,* vol. 9, No.3, pp. 217-243, 1995.